Received April 2001
Accepted March 2002

A numerical study of cavitation foot-prints in liquid-lubricated asymmetrical herringbone grooved journal bearings

Wan Junmei, T.S. Lee, C. Shu and Wu Jiankang
C/o Mechanical Engineering Department, National University of Singapore, Singapore

Keywords *Bearings, Fluid flow*

Abstract *A numerical model is presented in this paper to better describe the cavitated fluid flow phenomena in liquid-lubricated Asymmetrical Herringbone Grooved Journal Bearings (HGJBs). An effective "follow the groove" grid transformation method is used in the present study to capture all the groove boundaries. A singularity at the groove edges is avoided with this approach. Symmetrical groove patterns as well as asymmetrical groove patterns can be accurately computed with the proposed method. The difficult problem of abrupt changes of oil film thickness in the liquid-lubricated HGJB physical domain is modeled here through a series expansion approach. Results are comparable with available experimental and known numerical data from other investigators. Cavitation footprints, pressure distributions and their corresponding load characteristics are presented in this study. Effects of the critical transitional flow phenomena on the performance of the asymmetrical HGJBs are also determined through the present study.*

Nomenclature

c = radial clearance
e = eccentricity
h = film thickness
$\bar{h}$ = dimensionless film thickness (h/c)
H_g = groove depth
h_g = dimensionless groove depth (H_g/c)
g = switch function
i = subscript denoting circumferential direction
j = subscript denoting axial direction
J = Jacobian of transformation
J^{-1} = $1/J$
L/D = length to diameter ratio
$L_{1,2,3,4}$ = groove lengths as shown in Figure 1 (c)
P = film pressure
$\bar{P}$ = dimensionless film pressure $(P/\omega\mu)(c/R)^2$
P_a = ambient pressure
$\overline{P_a}$ = dimensionless ambient pressure
P_c = cavitation pressure
$\overline{P_c}$ = dimensionless cavitation pressure
R = bearing radium
t = time
$\bar{t}$ = dimensionless time (ωt)
U = journal surface velocity
W = load capacity
$\bar{W}$ = dimensionless load capacity $(W/\omega\mu R^2)\ (c/R)^2$
w_g = groove width
w_r = groove ridge width
x = coordinate in circumference
$\bar{x}$ = dimensionless of $x(x/2\pi R)$
y = coordinate in axial direction
$\bar{y}$ = dimensionless of $y(y/L)$
α = groove angle

International Journal of Numerical Methods for Heat & Fluid Flow, Vol. 12 No. 5, 2002, pp. 518-540.

DOI 10.1108/09615530210434278

β = bulk modulus
$\bar{\beta}$ = dimensionless bulk modulus $(\beta/\omega\mu)(c/R)^2$
ε = eccentricity ratio (e/c)
η,ξ = axes in computational domain
θ = density ratio (ρ/ρ_c)
μ = lubricant viscosity
ρ = fluid density
ρ_c = fluid density in cavitaion zone
ϕ = attitude angle
φ = circumferential coordinate [rad]
ω = angular rotation speed

1. Introduction

Cavitation footprints which may consist of gas or vapor or both have important influence on liquid-lubricated bearing behavior. The formation of cavities and their disposition affects the pressure distribution and hence the integrated quantities such as load capacity and attitude angle of bearings. When cavitation collapse, cavitation erosion (Dowson and Taylor, 1979) may occur and cause a variety of damage to the bearings. Various cavitation boundary conditions have been proposed by earlier researchers, such as the Sommerfeld conditions, half-Sommerfeld conditions (or Gumbel conditions), Reynolds conditions (or Swift-Stieber conditions) and JFO conditions. Half-sommerfeld conditions implies film rupture at the minimum film-thickness position and simply replaces the predicted negative pressure with zero. Reynolds condition is more precise than half- Sommerfeld conditions. It properly treats the film rupture but neglects the film reformation. JFO theory is regarded as one of the best theories that account for cavitation boundary conditions for hydrodynamic liquid lubrication. Elrod and Adams (1974) proposed a computational scheme that automatically implements JFO theory. Brewe (1986) modeled vaporous cavitation in dynamically loaded journal bearings using Elrod's algorithm. Vijayaraghavan and Keith (1989) proposed an improved scheme as an alternative to that of Elrod's algorithm. Vijayaraghavan and Keith (1990) modified their algorithm through grid transformation and adaptation techniques.

Herringbone grooved journal bearings (HGJBs) are frequently used in the computer HD, CD, VCD as well as DVD drives. Compared to plain journal bearings, HGJBs have much higher stiffness and stability characteristics. The slanted grooves pump the lubricants inward to achieve a higher pressure field in the center which will reduce cavitation as well as the leakage. Groove types can be designed for various purposes. Kawabata *et al.* (1989) proposed a regular and reversible rotation type. Chen (1995) suggested a self-replenishing asymmetrical hydrodynamic bearing. Typical asymmetrical HGJBs are shown in Figure 1.

The study of cavitation was neglected in HGJBs analysis till recently. Elrod's cavitation algorithm has been introduced into HGJBs by Jang and Chang (2000) (finite volume method) and Wu (2000) (operator-splitting method). However, their methods of applying symmetrical boundary conditions at groove apex are limited to only symmetrically grooved patterns.

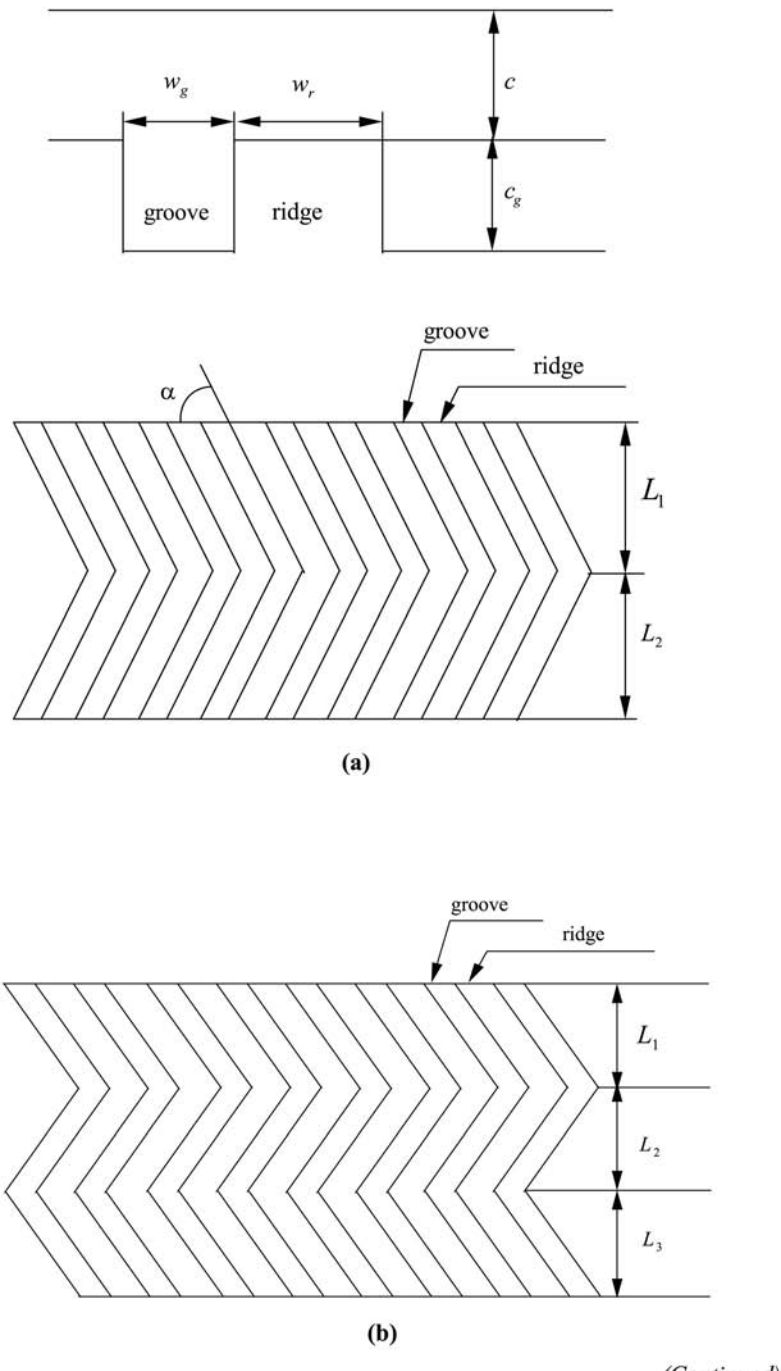

Figure 1.
Geometry and groove patterns of herringbone grooved journal bearings

(Continued)

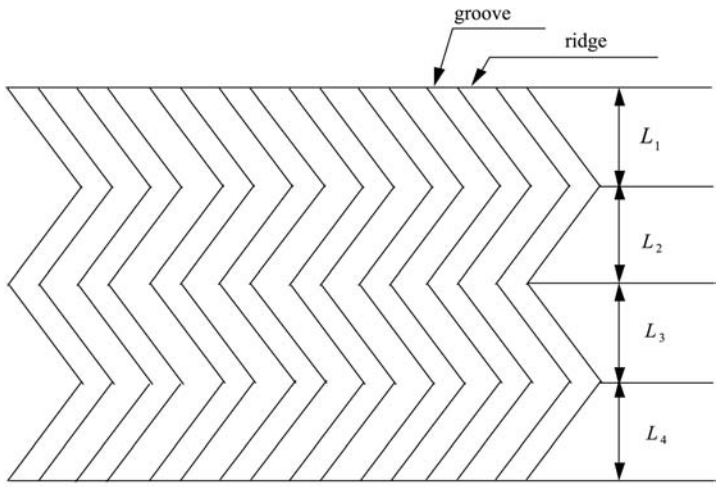

Figure 1.

The groove steps on either the journal or the sleeve create a discontinuity in the fluid film thickness that add difficulties in numerical solutions. The narrow groove theory (NGT) treats the groove-ridge pair as a control volume and assumes that since the number of grooves approaches infinity, the pressure distribution along the groove-ridge pair can be regarded as linear. Numerous researchers have worked concentrated on NGT, which matches the test data accurately only at low journal eccentricities and large number of groove-ridge pairs.

Several studies were accomplished for finite groove numbers in liquid-lubricated HGJBs. Bonneau and Absi (1994) determined the performance characteristics of gas-lubricated HGJBs with small number of rectangular-profile groove-ridge pairs by use of finite element method. Kang *et al.* (1996) deduced a finite difference method on 8 circular profile grooves. Zirkelback and Andres (1998) also detailed a finite element analysis on HGJBs.

There are no details reported on how to overcome the difficulties of film thickness discontinuities on small groove number HGJBs except Kang *et al.* (1996) mentioned that nodes are staggered to avoid these difficulties. In Jang and Chang (2000), 200 grid points in the circumferential direction obviously cannot catch all the 16 groove-ridge interfaces.

The present study incorporates Elrod's algorithm with Reynolds equation to predict the cavitation zone and other static characteristics of asymmetrical HGJBs. A Grid transformation technique is applied along the groove direction

over the entire solution domain. Groove apex singularity at the groove center, groove ridge interfaces and abrupt film thickness changes are considered in the present work. Results are compared with available published symmetrical groove pattern and the reversible one groove patterns are compared with the work of Kawabata *et al.* (1989).

2. Analytical model and numerical methods

2.1 Problem formulation

For the present problem, the oil "groove" is considered as the static member, while the "smooth" shaft is considered as the rotational member. The governing, two dimensional, Reynolds equation, describing the laminar flow for a Newtonian lubricant with compressibility effects, can thus be written as:

$$\frac{\partial \rho h}{\partial t} + \frac{\partial}{\partial t}\left(\frac{\rho h U}{2} - \frac{\rho h^3}{12\mu}\frac{\partial P}{\partial x}\right) + \frac{\partial}{\partial y}\left(-\frac{\rho h^3}{12\mu}\frac{\partial P}{\partial y}\right) = 0. \tag{1}$$

Elrod (1974), Elrod (1981) modified this equation by introducing a switch function g in order to automatically implement the cavitation boundary conditions. In the cavitation zone, $g = 0$; in the full film zone, $g = 1$. Thus, the pressure flow within the cavitation zone can be switched on and off in the groove domain with mass conservation according to JFO theory,

$$\frac{\partial \rho_c h\theta}{\partial t} + \frac{\partial}{\partial x}\left(\frac{\rho_c h U}{2}\theta - \frac{\rho_c \beta h^3 g}{12\mu}\frac{\partial \theta}{\partial x}\right) + \frac{\partial}{\partial y}\left(-\frac{\rho_c \beta h^3 g}{12\mu}\frac{\partial \theta}{\partial y}\right) = 0 \tag{2}$$

The density of the lubricant is related to the film pressure through the definition of the bulk modulus, β, and density ratio, θ, i.e.

$$g\beta = \rho\frac{\partial P}{\partial \rho} \tag{3}$$

$$\theta = \frac{\rho}{\rho_c} \tag{4}$$

Combining equations (3) and (4) and integrating yields

$$P = P_c + g\beta \ \ln\theta \tag{5}$$

After obtaining the solution of Equation (2) which gives us a value of θ, and using Equation (5), we will get pressure distribution in the whole domain.

Equation (2) can be nondimensionalized by using dimensionless variables as defined in the nomenclature,

$$\frac{\partial(\theta\bar{h})}{\partial\bar{t}}+\frac{1}{4\pi}\frac{\partial(\theta\bar{h})}{\partial\bar{x}}=\frac{\bar{\beta}}{48\pi^2}\frac{\partial}{\partial\bar{x}}\left(\bar{h}^3\frac{\partial\theta}{\partial\bar{x}}\right)+\frac{\bar{\beta}}{48(L/D)^2}\frac{\partial}{\partial\bar{y}}\left(\bar{h}^3\frac{\partial\theta}{\partial\bar{y}}\right) \quad (6)$$

For simplicity, the bar notation "-" will be dropped in the following analysis.

While the switch function is not explicitly differenced, we may write that $g(\partial\theta/\partial x)=(\partial g(\theta-1)/\partial x)$ Vijayaraghavan and Keith (1989).

Combining the above with Equation (6) produces,

$$h\frac{\partial\theta}{\partial t}+\frac{1}{4\pi}\left(h\frac{\partial\theta}{\partial x}+\theta\frac{\partial h}{\partial x}\right)=\frac{\beta}{48\pi^2}\left\{h^3\frac{\partial}{\partial x}\left(\frac{\partial g(\theta-1)}{\partial x}\right)+3h^2\cdot\frac{\partial h}{\partial x}\cdot\frac{\partial g(\theta-1)}{\partial x}\right\}$$

$$+\frac{\beta}{48(L/D)^2}\left\{h^3\frac{\partial}{\partial y}\left(\frac{\partial g(\theta-1)}{\partial y}\right)+3h^2\cdot\frac{\partial h}{\partial y}\cdot\frac{\partial g(\theta-1)}{\partial y}\right\} \quad (7)$$

2.2 Grid transformation

In order to model the complex geometry of groove patterns and to simplify the computations, the grids that are arranged along the slant grooves in the x-y physical domain will be transformed to $\xi-\eta$ computational domain. The x direction is taken as ξ direction and the groove direction as η direction.

Thus,

$$\eta_x=0, f_x=\frac{\partial f}{\partial x}=\xi_x\frac{\partial f}{\partial\xi}+\eta_x\frac{\partial f}{\partial\eta}=\xi_x\frac{\partial f}{\partial\xi}$$

$$f_y=\frac{\partial f}{\partial y}=\xi_y\frac{\partial f}{\partial\xi}+\eta_y\frac{\partial f}{\partial\eta}$$

$$\xi_x=J^{-1}y_\eta;\ \eta_x=J^{-1}y;\ \xi_y=J^{-1}x_\eta;\ \eta_y=J^{-1}x_\xi$$

$$J=x_\xi y_\eta-x_\eta y_\xi$$

Equation (7) can be written in the computational domain as,

$$h\frac{\partial\theta}{\partial t}+\frac{1}{4\pi}\left(h\frac{\partial\theta}{\partial\xi}+\theta\frac{\partial h}{\partial\xi}\right)\cdot\xi_x=\frac{\beta}{48\pi^2}\left\{h^3\frac{\partial}{\partial\xi}\left(\frac{\partial g(\theta-1)}{\partial\xi}\right)\right.$$
$$\left.+3h^2\frac{\partial h}{\partial\xi}\cdot\frac{\partial g(\theta-1)}{\partial\xi}\right\}\cdot\xi_x^2+\frac{\beta h^3}{48(L/D)^2}\left\{\frac{\partial}{\partial\xi}\left(\xi_y\cdot\frac{\partial g(\theta-1)}{\partial\xi}\right.\right.$$
$$\left.+\eta_y\cdot\frac{\partial g(\theta-1)}{\partial\eta}\right)\cdot\xi_y+\frac{\partial}{\partial\eta}\left(\xi_y\cdot\frac{\partial g(\theta-1)}{\partial\xi}+\eta_y\cdot\frac{\partial g(\theta-1)}{\partial\eta}\right)\cdot\eta_y\Bigg\} \tag{8}$$
$$+\frac{\beta h^2}{16(L/D)^2}\left\{\xi_y^2\cdot\frac{\partial h}{\partial\xi}\cdot\frac{\partial g(\theta-1)}{\partial\xi}+\eta_y\cdot\xi_y\cdot\frac{\partial h}{\partial\eta}\cdot\frac{\partial g(\theta-1)}{\partial\xi}\xi_y\cdot\eta_y\cdot\frac{\partial h}{\partial\xi}\cdot\frac{\partial g(\theta-1)}{\partial\eta}\right.$$
$$\left.+\eta_y^2\cdot\frac{\partial h}{\partial\eta}\cdot\frac{\partial g(\theta-1)}{\partial\eta}\right\}$$

2.3 Treatment of the groove apex

Along the apex of grooves when groove edges change direction, there is a singularity in ξ_x since the values on the upper and lower part of this line are constants but have opposite signs. A symmetrical boundary condition $\partial\theta/\partial y$ is often used in literature to avoid this singularity and simplify the grid transformation, i.e. the transformation is used only within the half domain. However, these methods are limited to symmetrical problems and have to handle Neumann boundary conditions. To remedy this, an innovative method is applied here. The coordinate transformation is performed over the entire domain and the ξ_x value on the apex line is assumed to be the average ξ_x of the upper and lower grid values which are next to the apex grids. Thus, the method can be readily applied to asymmetrical groove patterns and only Dirichlet boundary conditions are needed.

2.4 Lubricant film thickness

The film thickness is known as:

$$h=f(\xi)+h(x)$$

$$h(x)=1+\varepsilon\cos(\varphi)$$

$$\varphi=2\pi x$$

$$f(\xi)=\left.\begin{matrix}0\ \ on\ \ the\ \ ridge\\ h_g\ \ in\ \ the\ \ groove\end{matrix}\right\}$$

$$\frac{\partial h}{\partial \xi} = f'(\xi) + h'(x) \cdot x_{\xi} \tag{9}$$

$$\frac{\partial h}{\partial \eta} = h'(x) \cdot x_{\eta} \tag{10}$$

$$h'(x) = -2\varepsilon \sin(\varphi) \tag{11}$$

2.5 Load capacity and attitude angle

The radial and tangential loads (forces acting along and normal to the line of center, respectively) can be determined after the pressure is obtained within the fluid film as,

$$F_{\theta} = \iint_{s} P \sin\theta \mathrm{d}x\mathrm{d}y \tag{12}$$

$$F_{r} = -\iint_{s} P \cos\theta \mathrm{d}x\mathrm{d}y \tag{13}$$

Load capacity and attitude angle can then be determined as follows:

$$W = \sqrt{F_r^2 + F_{\theta}^2} \tag{14}$$

$$\phi = \tan^{-1}(F_{\theta}/F_r) \tag{15}$$

The dimensionless load capacity is defined for parametric study as the nomenclature.

2.6 Numerical formulations

Since at present stage we consider only steady problems, we will set the groove member as the static member, while the smooth member as the rotating member.

Equation (8) is discretized using a finite-difference method. The shear flow term is discretized by a second order upwind scheme:

$$\frac{1}{4\pi}\left(h\frac{\partial \theta}{\partial \xi}\right) \cdot \xi_x|_{i,j} = \frac{h_{i,j}}{4\pi} \frac{3\theta_{i,j} - 4\theta_{i-1,j} + \theta_{i-2,j}}{2\Delta\xi} \cdot \xi_{xi,j} \tag{16}$$

Other terms were discretized by central-difference schemes.

The film thickness at abrupt changes must be carefully treated. The derivative of h need not be discretized since the exact values can be given. Though, at the groove-ridge boundaries, $\partial h/\partial \xi$ is theoretically infinite and is modeled here as,

Method-a: We assume the steep groove-ridge boundary as a slope. It is reasonable to make such assumption since real flow cannot be infinite steep along a real wall due to viscosity.

$$f'(\xi) = \left\{ \begin{array}{ll} \pm \dfrac{h_0}{2\Delta\xi} & at\ groove - ridge\ boundaries \\ 0 & other\ places \end{array} \right\} \tag{17}$$

Method-b: After all the grids are arranged to catch the groove-ridge boundaries, a translation of all the grid in the ξ direction for half of $\Delta\xi$, so that no grid will be at groove-ridge boundaries. The difficulty of abrupt changes in film thickness is thus avoided totally.

The above equations are solved by using an explicit method in conjunction with a 4-level Runge-Kutta algorithm. A total of 129 nodes were used in the circumferential direction and 21 nodes were used in the axial direction. To obtain the steady – state solution, a time march is performed until the convergence criteria are achieved.

$$\theta^{n+1} = \theta^n + \mathrm{Re}\ sidual{\cdot}\Delta t \ \text{(n denoting time level)}$$

$$\max_{i,j} |\mathrm{Re}\ sidual| \le 10^{-4}$$

Time step is chosen based on CFL conditions and can be roughly expressed as,

$$\Delta t = \lambda{\cdot}\frac{24\pi^2}{\beta h_{\max}^3}{\cdot}\Delta x{\cdot}\Delta y$$

λ is a constant chosen as 0.5 presently so that a convergence can be achieved.

3. Validations and comparison

3.1 Comparison of method-a and method-b

Pressure distributions obtained by method-a and method-b using data given by Jang and Chang (2000) in Table I are shown in Figure 2. Method-a presents a saw-tooth shaped pressure distribution while method-b presents a smooth one. Zirkelback and Andres (1998) mentioned that around the circumference of the bearing, a saw-tooth shaped pressure gradient resulted due to the varying clearances that occurred with alternating grooves and ridges. Saw-tooth shaped pressure distribution can be also found in Bonneau and Absi (1994) for an aerodynamic journal bearing and in Jang and Chang (2000) for a hydrodynamic journal bearing with small number of herringbone grooves. Method-a is deemed as more reasonable because it presents results that are in agreement with earlier reports. Therefore, we will apply method–a to further analysis.

3.2 Validations

Results obtained from the analysis detailed above are first compared with experimental data for the symmetrical herringbone grooved journal bearing investigated by Hirs (1965). Geometry and operating conditions are given in Table I. The agreement was quite good using the same parameters given by Jang and Chang (2000) and the comparison is shown in Figure 2. Figure 3 shows a comparison of the dimensionless load capacity, as presented by Kawabata *et al.* (1989), to the present numerical predictions. As shown in the figure, the predicted load capacity by present numerical method agrees well with that of Kawabata *et al.* at small eccentricities. It is noticed that there are

	Kawabata *et al.* (1989)	Jang and Chang (2000)
Number of grooves	8	8
L/D	2.0	1.0/2.0
$\bar{\beta}$	23854	23854
h_g	1.0	1.0
α	30[deg.]	70[deg.]
w_g/w_r	1.0	1.0
P_a^-	0.0	
P_c^-	−0.1	

Table I.
Geometry and operating conditions of a reversible herringbone grooved Journal bearing

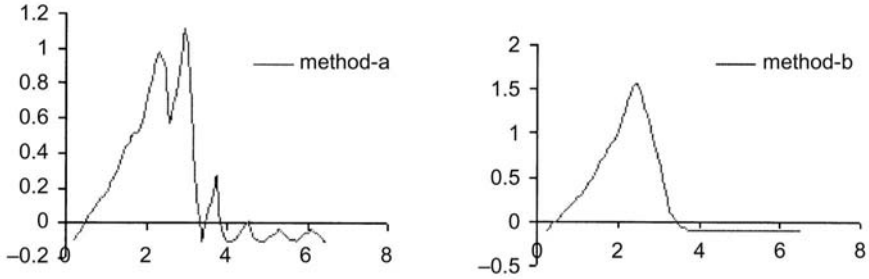

Figure 2.
Pressure distribution (dimensionless) along circumference at axial position from centerline (L/5D)

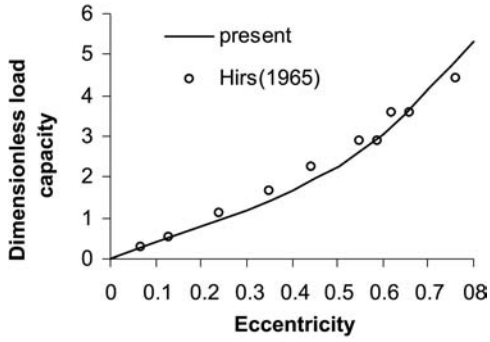

Figure 3.
Comparison of dimensionless load capacity with experimental result of Hirs (1965)

some discrepancy at large eccentricities. The discrepancy might due to negligence of cavitation in Kawabata *et al.* analysis because cavitation occurs at large eccentricities.

4. Results and discussions

4.1 Effects of eccentricity and groove length ratio on cavitation zones

The cavitation zones of asymmetrical herringbone journal bearings with different eccentricities and groove length ratios are shown in Figure 5. Cavitation generally develops at the diverging section of asymmetrical HGJBs and follows the groove shape as the groove apex moves. The cavitation area decreases with decreasing eccentricity.

4.2 Variation of cavitation zones with dimensionless groove depth, groove angle, L/D and dimensionless cavitation pressure

Figure 6 shows that the variation of cavitation area due to dimensionless groove depth, groove angle, L/D and dimensionless cavitation pressure for an asymmetrical HGJB at groove length ratio $L1 : L2 = 7 : 3$. At large eccentricity, with the increasing of dimensionless groove depth, groove angle, L/D ratio and cavitation pressure, the cavitation area increases. At small eccentricity where is defined here to be less than 0.6, no cavitation is found.

4.3 Pressure distribution variations with groove length ratio

Figure 7 (1) shows the pressure distribution of predicted pressure in the along axial direction at $x = 0.5888$. The peak pressure moves to the position of groove apex while the groove apex moves. Comparing to a symmetrical grooved bearing, pressure distributions of asymmetrical HGJBs axial direction are asymmetrical while those of symmetrical ones are symmetrical. At one end,

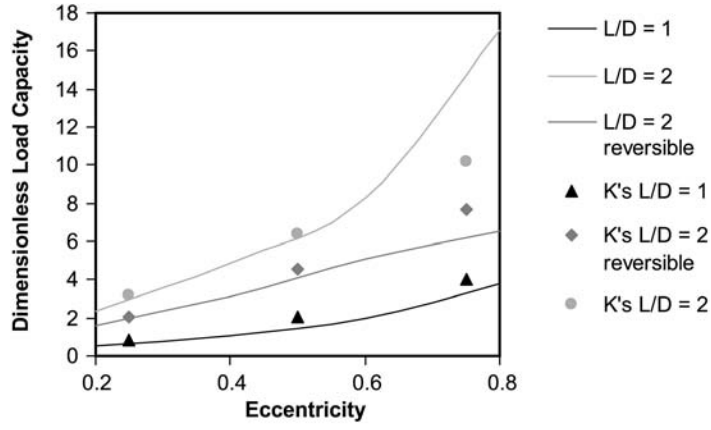

Source: "K's" stands for Kawabata *et al.* (1989)'s result

Figure 4.
Dimensionless load capacity compared with Kawabata *et al.* (1989)'s data. ("K's" stands for Kawabata *et al.* (1989)'s result)

(a) L1/L2 = 3:7, *Pc* = –0.1, ε = 0.6

(b) L1/L2 = 3:7, *Pc* = –0.1, ε = 0.8

(c) L1/L2 = 3.5:6.5, *Pc* = –0.1, ε = 0.6

(d) L1/L2 = 3.5:6.5, *Pc* = –0.1, ε = 0.8

(e) L1/L2 = 4:6, *Pc* = –0.1, ε = 0.6

(f) L1/L2 = 4:6, *Pc* = –0.1, ε = 0.8

(*Continued*)

Figure 5.
Cavitation zone variance due to eccentricity and groove length ratio

(g) L1/L2 = 4.5:5.5, *Pc* = –0.1, ε = 0.6

(h) L1/L2 = 4.5:5.5, *Pc* = –0.1, ε = 0.8

(i) L1:L2:L3 = 1:2:1, *Pc* = –0.1, ε = 0.6

(j) L1:L2:L3 = 1:2:1, *Pc* = –0.1, ε = 0.8

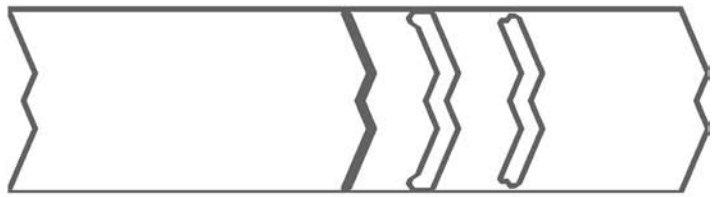

(k) L1:L2:L3:l4 = 7:3:3:7, L/D = 2, *Pc* = –0.1, ε = 0.6

(l) L1:L2:L3:L4 = 7:3:3:7, L/D = 2, *Pc* = –0.1, ε = 0.8

Figure 5.

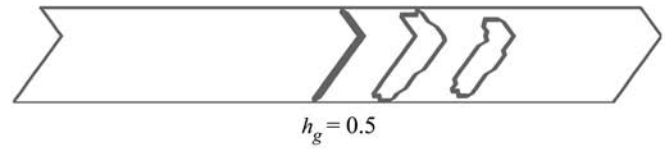

$h_g = 0.5$

$h_g = 0.9$

$h_g = 1.5$

(1) Cavitation zone variance due to dimentionless groove depth h_g when $Pc = 0.1$, $\varepsilon = 0.6$

L/D = 0.5

L/D = 1.0

L/D=2.0

(2) Cavitation zone variance due to L/D ratio when $Pc = 0.1$, $\varepsilon = 0.6$

(*Continued*)

Figure 6.
Cavitation zone variance due to different geometry and operation conditions when L1/L2 = 7 : 3 for groove type (a)

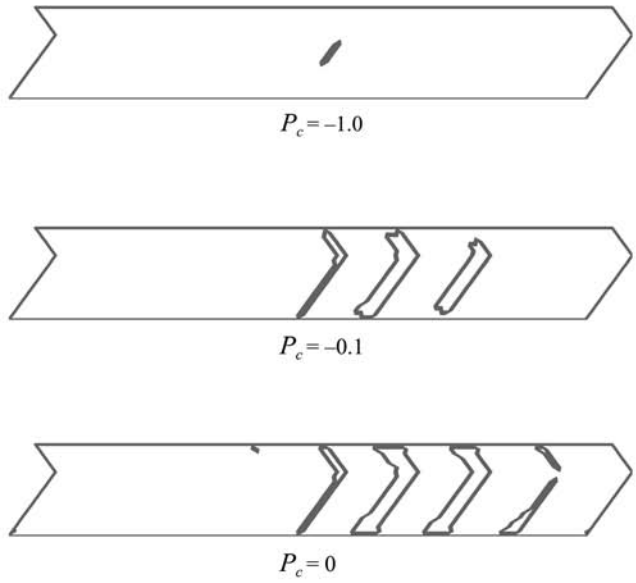

(3) Cavitation zone variance due to cavitation pressure P_c when ε = 0.6, L/D = 1

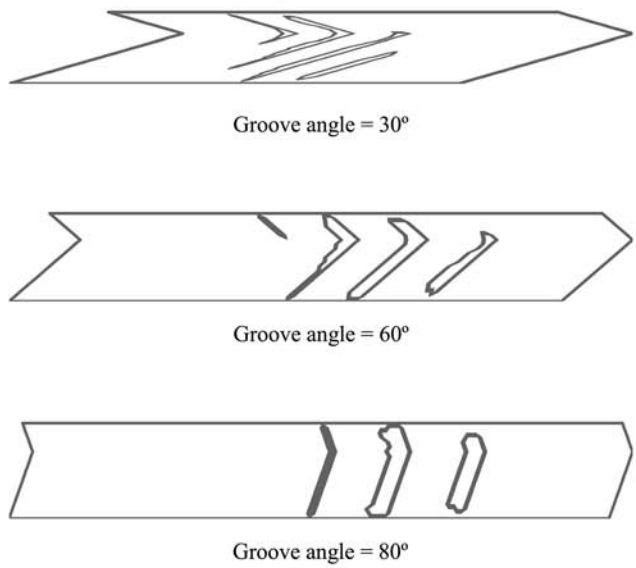

(4) Cavitation zone variance due to groove angle when $Pc = -0.1$, ε = 0.6

Figure 6.

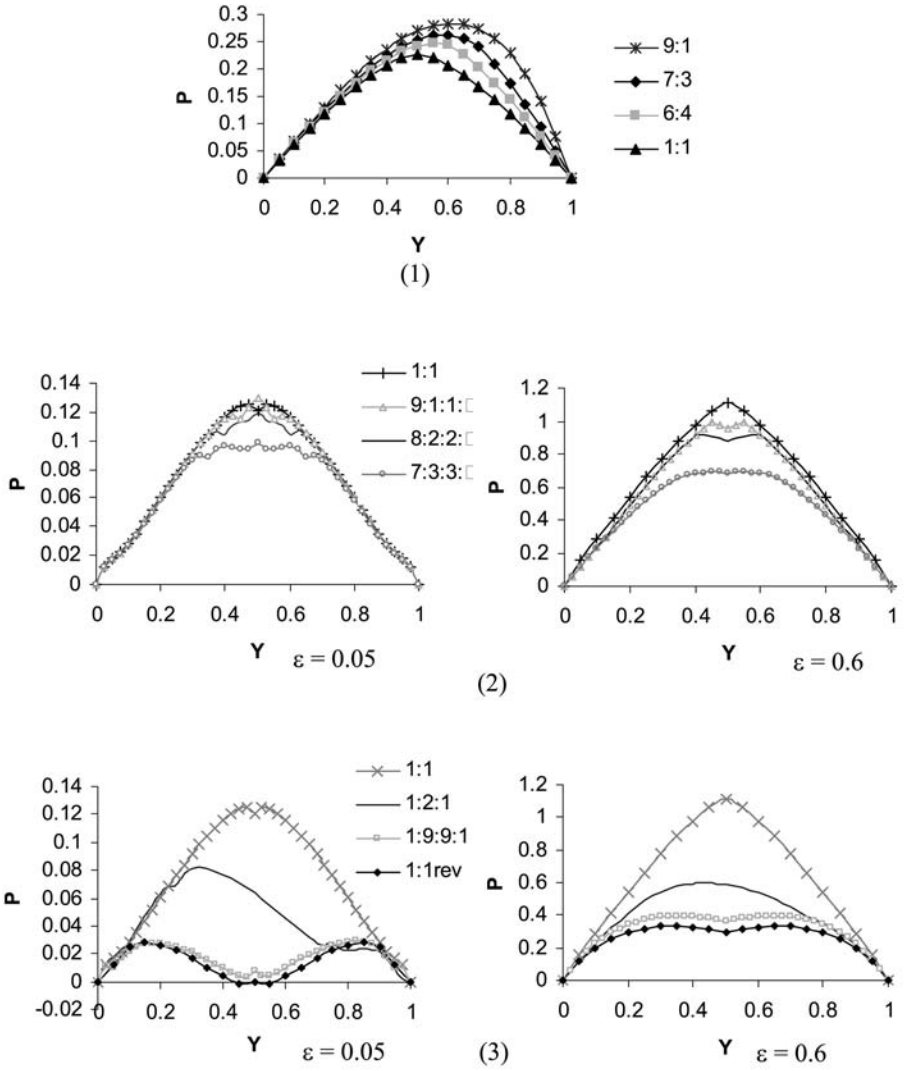

Figure 7.
Pressure distribution along grooves at $x = 0.5888$. (1) for Type (a): L/D = 1, $\varepsilon = 0.6$; (2) for Type (c): L/D = 2; (3) for Type (a), (b) and (c): L/D = 2

$\partial P/\partial y$ decreases while at the other end it increases. As we known, axial leakage rate is proportional to pressure gradient at both ends of the bearing. Thus, asymmetrical groove pattern can increase leakage at one end and decrease leakage at the other end. As the groove length ratio increases, the leakage difference at both ends increases. A proper ratio can be found at which zero-leakage can be achieved considering surface tension and gravity.

The pressure distributions along axial direction when $x = 0.5888$ for HGJBs of Type (c) are presented in Figure 7 (2). The pressure distributions are

symmetric since the groove pattern chosen here are symmetric along the groove center. Unlike a symmetrical HGJB of Type (a), the peak pressure of a HGJB of Type (c) does not occur at the line of groove center, but occurs near the line of upper and the lower apex. Leg AB and BC form a herringbone groove that pumps lubricant toward B while leg CD and DC form another that pumps lubricant toward D. Figure 4 and 5 (2) shows that groove patterns with longer BC and DC have less pumping effect and result in lower peak pressure. It is because the herringbone groove formed by leg BC and CD does not contribute to the pumping effect. As shown in Figure 4 and 5 (2), when $\varepsilon = 0.6$, the pressure distributions of groove length ratios of 1:1, 9:1:1:9 and 8:2:2:8 are very close to one another. It reveals that though the pumping effects are closely related to groove length ratios, they are not simply proportional to groove length ratios.

Figure 7 (3) compares pressure distributions of HGJBs of Type (a), (b) and (c) when $L/D = 2$. A groove length ratio of 1:1 forms a HGJB of Type (a). When it rotates in an opposite direction, it is named as '1:1 rev'. A groove length ratio of 1:9:9:1 is a HGJB of Type (c). Its leg BC and CD are so long that it is similar to the '1:1 rev' groove pattern, as most of its groove parts, BC and CD cannot achieve to pumping effects. A groove length ratio of 1:2:1 represents a HGJB of Type (b). It is shown in Figure 4 and 5 (3) that the peak pressure of a HGJB with groove length ratio of 1:1 is the highest. The HGJB of '1:1 rev', which rotate in opposite direction, produces lowest peak pressure. When $\varepsilon = 0.05$, the pressure is so close to zero that it reaches negative at apexes. This reveals that the pumping force of a HGJB might be lost when it rotates in opposite direction at near-concentric conditions. The design of reversible HGJBs of Type (b) is necessary since journal bearing will be very unstable and half-frequency whirl may occur without the pumping force at near-concentric conditions. The peak pressure of a reversible HGJB with groove length ratio of 1:2:1 is 50 per cent to 70 per cent of what produced by the normal HGJB with groove length ratio of 1:1. It is because only part of the groove of 1:2:1 contributes to the pumping effect. However, it can avoid a very unstable condition when a normal HGJB accidentally rotates in the wrong direction.

4.4 Effect of groove length ratio of type (a) HGJBs on dimensionless load capacity and attitude angle

Figure 8 demonstrates the dimensionless load capacity and attitude angle variance due to groove length ratio. Values of dimensionless load capacity and attitude angle at different groove length ratios are given in Table II. It is shown that the dimensionless load capacity decreases, the attitude angle increases with an decreasing of L2, i.e. an increasing of L1:L2 ratio, since $L1 + L2 = 1.0$. The maximum load capacity and minimum attitude angle are obtained when L2 equals 0.5 which is a symmetrical groove pattern. Hence, we can conclude that the symmetrical groove pattern can achieve the best stability and load

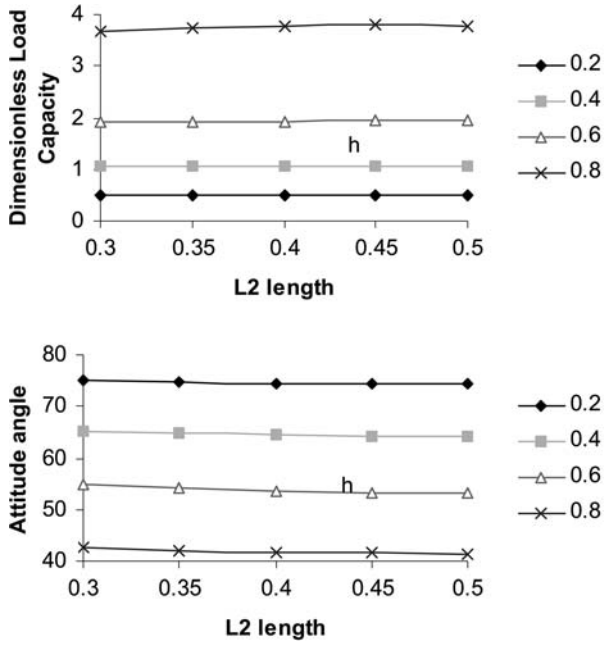

Figure 8.
Dimensionless load capacity and attitude angle variance due to groove length ratio for groove type (a), L1 + L2 = 1.0

capacity. However, the differences of dimensionless load capacity and attitude angle are so small that they might be negligible in most cases.

4.5 Effect of groove geometry on dimensionless load capacity and attitude angle
Figure 9 gives the change of the dimensionless load capacity and attitude angle due to different groove geometry when groove length equals 7:3. We can see from Figure 9 that with an decreasing of groove depth, an increasing of L/D ratio, the load capacity increases. For small eccentricity which implies a near-concentric condition, the smallest attitude angle occurs at a groove depth of 0.9, a L/D ratio 1.0 and a groove angle of 40°. A groove angle of 40° also achieves maximum dimensionless load capacity at a small eccentricity which is less than 0.1. The load capacity slightly increases and the attitude angle decreases with an increasing of groove angle at large eccentricities.

L1:L2	$\bar{W}$	ϕ
7:3	1.906323	54.85221
6.5:3.5	1.917753	54.24816
6:4	1.930523	53.71764
5.5:4.5	1.941192	53.37064
5:5	1.952863	53.2018

Table II.
Dimensionless load capacity and attitude angle for different groove length ratio at eccentricity = 0.6

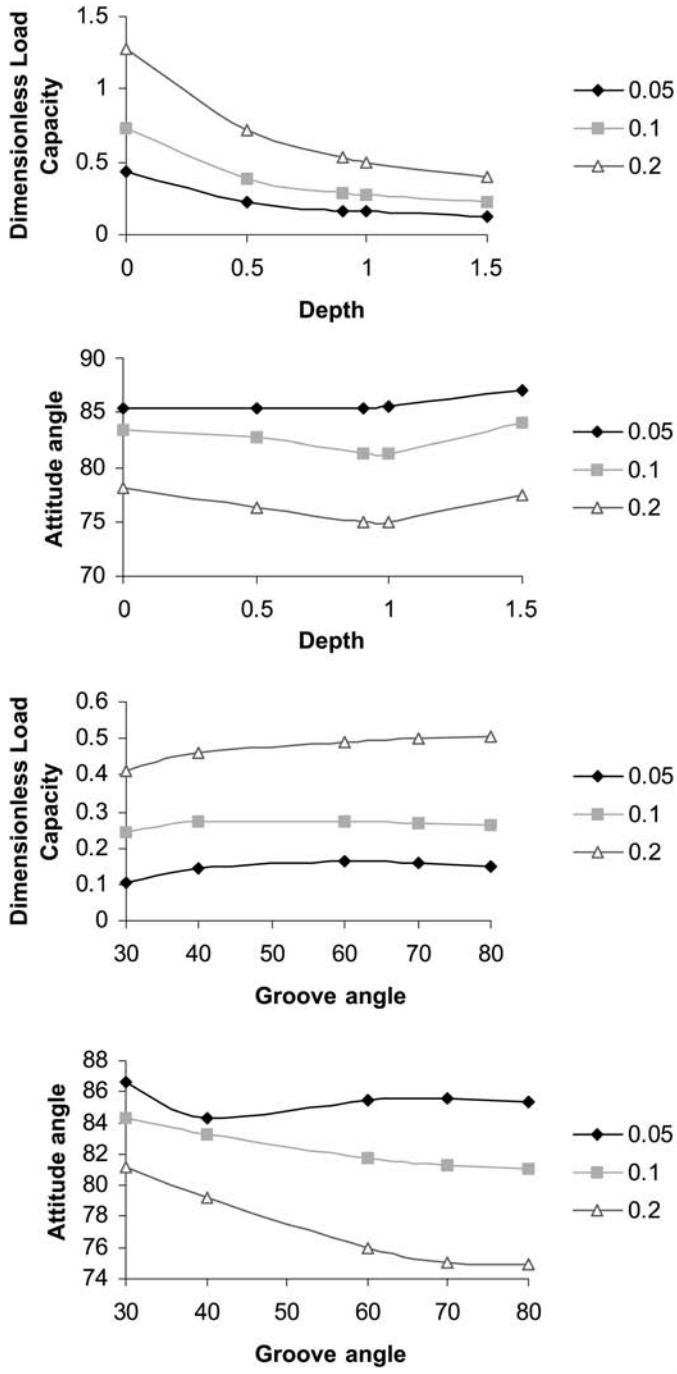

Figure 9.
Dimensionless load capacity and attitude angle variance due to geometry of asymmetrical HGJBs when groove length ratio L1 : L2 = 7 : 3 at various eccentricity ratios

(*Continued*)

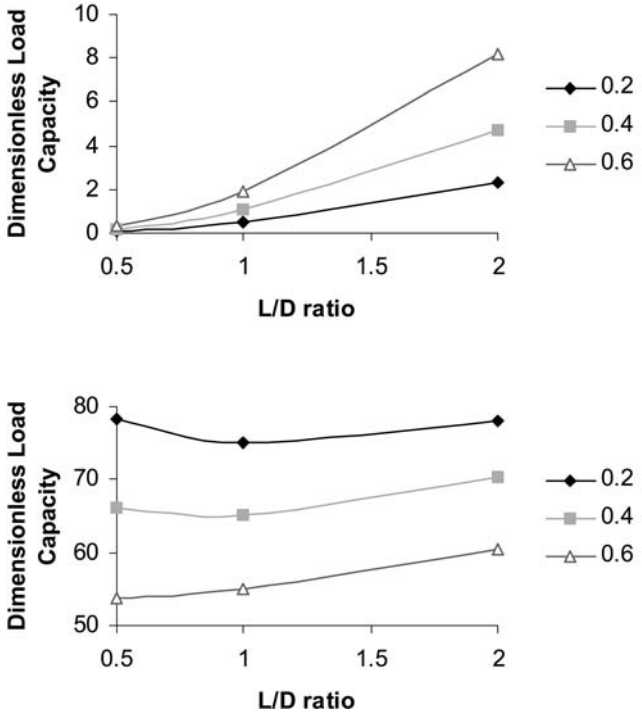

Figure 9.

4.6 Dimensionless load capacity and attitude angle vary with dimensionless cavitation pressure

Figure 10 presents the variation of the dimensionless load capacity and attitude angle with the dimensionless cavitation pressure when the groove length ratio equals 7:3. The dimensionless load capacity and the attitude angle decreases as the cavitation pressure increases. The pressure difference before and after the position of minimum film thickness is larger when the cavitation pressure is smaller. Hence, the load capacity, which is an integrated value, is larger. On the other hand, for a case when the cavitation pressure equals -1.0, it is very unstable since the attitude angle is very close to 90° even for a large eccentricity of 0.6. It might because that there is not much cavitation occur till an eccentricity of 0.6. Consequently, the pressure profile of the journal bearing remains antisymmetrical about the position of minimum film thickness, and results in a large attitude angle and unstable condition. Again, the significant effect of cavitation on journal bearing performance is proved.

5. Conclusions

This paper presented cavitation footprints of asymmetrical herringbone grooved journal bearings. The effects of groove –ridge interface geometry was

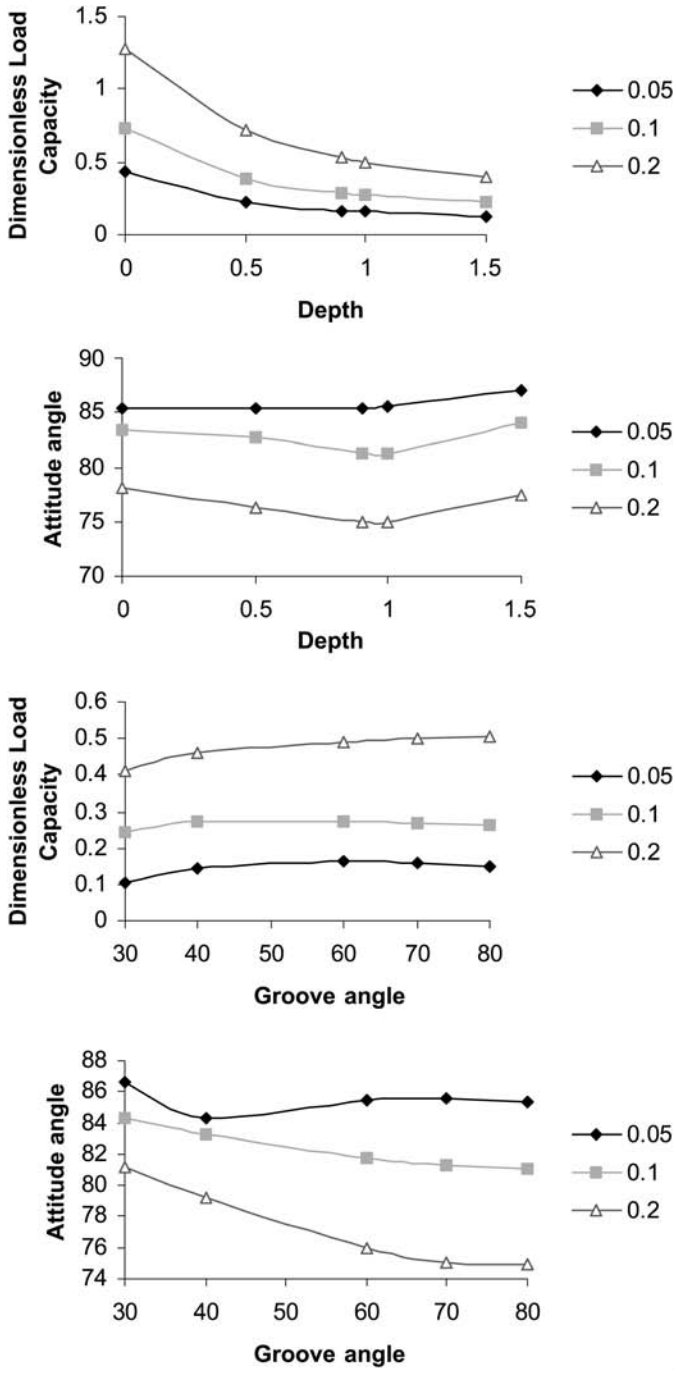

Figure 10.
Dimensionless load capacity and attitude angle variance due to dimensionless cavitation pressure of asymmetrical HGJBs when groove length ratio L1 : L2 = 7 : 3

(*Continued*)

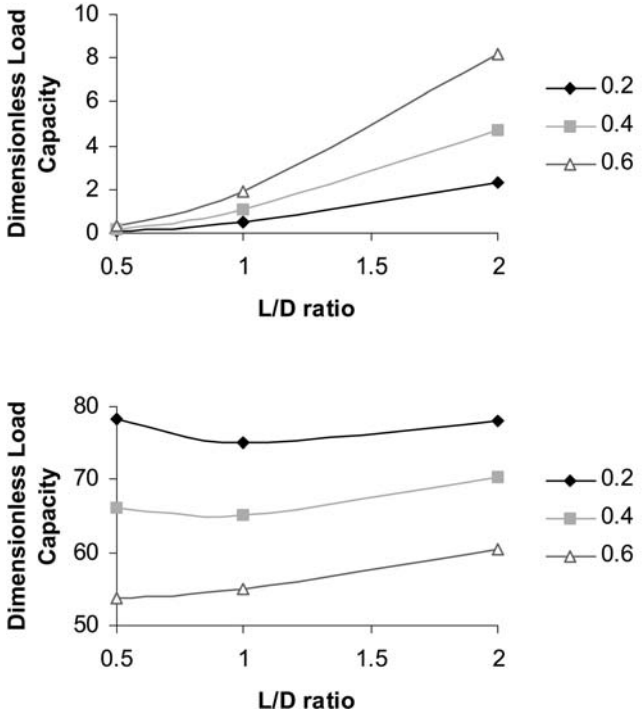

Figure 10.

considered. The results indicate that the cavitation area follow the shape of groove as the groove shape changes. The cavitation area decreases with the increasing of L/D ratio, groove angle and dimensionless cavitation pressure, and the decreasing of dimensionless groove depth ratio. The load capacity and attitude angle of a type (a) asymmetrical HGJB are not greatly different from those of a symmetrical HGJB. The load capacity decreases, the attitude angle increases slightly as the groove length ratio increases. Though Type (b) HGJB has inferior pumping effect than a symmetrical HGJB, it can avoid an extremely unstable condition when a symmetrical HGJB rotates in a wrong direction. The pumping effect of a Type (c) HGJB is found to be related to the groove length ratio, but not proportional to it. The effects of cavitation on the performance of a type a asymmetrical HGJB at a groove length ratio of 7:3 were also investigated. The load capacity increases as the L/D ratio increases and groove depth, cavitation pressure decrease. For small eccentricity, the minimum attitude angle is got when $h_g = 0.9$, L/D = 1.0, $\alpha = 40°$. Cavitation is proved to have great effect on performance of asymmetrical grooved journal bearing as well.

References

Brewe, D.E. (1986), "Theoretical modeling of the vapor cavitation in dynamically loaded journal bearings", *ASME Journal of Tribology*, Vol. 108, pp. 628-38.

Bonneau, D. and Absi, J. (1994), "Analysis of aerodynamic journal bearings with small number of herringbone grooves by finite element method", *ASME Journal of Tribology*, Vol. 116, pp. 698-704.

Chen, S.H. (1995), "Self-replenishing hydrodynamic bearing," United States Patent, Patent Number: 5, 407, 281.

Dowson, D. and Taylor, C.M. (1979), "Cavitation in bearings", Annual Review of Fluid Mechanics, pp. 35–66.

Elrod, H.G. (1981), "A cavitation algorithm", in, *ASME Journal of Lubrication Technology*, Vol 103, pp. 350-4.

Elrod, H.G. and Adams, M.L. (1974), "A computer program for cavitation and starvation problems", in, *Cavitation and Related Phenomena in Lubrication*, Mechanical Engineering Publications, New York pp. 37-41.

Hirs, G.G. (1965), "The load capacity and stability characteristics of hydrodynamic grooved journal bearings", *ASLE Transctions*, Vol. 8, pp. 296-305.

Jang, G.H. and Chang, D.I. (2000), "Analysis of hydrodynamic herringbone grooved journal bearing considering cavitation", *ASME Journal of Tribology*, Vol. 122, pp. 103-9.

Kang, K., Rhim, Y. and Sung, K. (1996), "A study of the oil-lubricated herringbone-grooved journal bearing—part 1: numerical analysis", *ASME Journal of Tribology*, Vol. 118, pp. 906-11.

Kawabata, N., Ozawa, Y., Kamaya, S. and Miyake, Y. (1989), "Static characteristics of the regular and reversible rotation type herringbone grooved journal bearing", *ASME Journal of Tribology*, Vol. 111, pp. 484-90.

Vijayaraghavan, D. and Keith, T.G. Jr. (1989), "Development and evaluation of a cavitation algorithm", *STLE Tribology Transactions*, Vol. 32 No. 2, pp. 225-33.

Vijayaraghavan, D. and Keith, G.T. Jr. (1990a), "An efficient, robust and time accurate numerical procedure applied to a cavitation algorithm", *ASME Journal of Tribology*, Vol. 112, pp. 44-51.

Vijayaraghavan, D. and Keith, T.G. Jr. (1990b), "Grid transformation and adaption techniques applied to the analysis of cavitated journal bearings", *ASME Journal of Tribology*, Vol. 112, pp. 52-9.

Wu Jiankang (2000), "Operator-splitting method to calculate film pressure of herringbone grooved journal bearing", *Pan-den Pre-research project of China National Science and Technology Committee (PD9521901)*, pp. 1-9.

Zirkelback, N. and Andres, L.S. (1998), "Finite element analysis of herringbone groove journal bearings: a parametric study", *ASME Journal of Tribology*, Vol. 120, pp. 234-40.